Synthesis of Mixed-Anion Fluorosulfide $Ba_{18}F_{18}In_8S_{21}$ and Comparison between Experimental and Theoretical Fluorine K-edge X-ray Absorption Near Edge Structure

Tomoki Tsukamoto[1], Shintaro Tachibana[1], Yuki Orikasa[1]

1) *Department of Applied Chemistry, College of Life Sciences, Ritsumeikan University, 1-1-1 Noji-Higashi, Kusatsu 525-8577, Japan*

Mixed-anion fluoride compounds containing highly polarizable sulfide ions are less widely reported than comparable single-anion materials and have potential use in device applications. This study reports the synthesis of $Ba_{18}F_{18}In_8S_{21}$ and its crystal structure analysis by X-ray diffraction and electronic structure analysis by fluorine K-edge X-ray absorption spectroscopy. The solid-phase synthesis of $Ba_{18}F_{18}In_8S_{21}$ using indium sulfide as starting material was superior to that using indium metal and elemental sulfur and yielded a product with comparatively little impurity. The experimental fluorine K-edge X-ray absorption near edge structure of $Ba_{18}F_{18}In_8S_{21}$ was well-reproduced by the first principles calculations using the CASTEP program.

1. Introduction

Single-anion compounds comprising oxides, sulfides, or fluorides are used primarily as functional materials for device applications. There are few comparable examples of compounds with multiple anions. However, mixed-anion compounds may be able to achieve greater functionality in the design of future materials.[1] Although reports of oxide-based mixed-anion compounds containing fluoride and nitride ions are increasing,[2-4] fluoride-based mixed-anion compounds have not been widely reported apart from oxyfluorides. This occurs because fluorides are sometimes difficult to work with relative to oxides, which are easily handled in the atmosphere. Many single-anion fluoride crystal structures have been reported.[5] Therefore, fluoride-based mixed-anion compounds should be a useful source of functional materials. This study focuses on the preparation and characterization of fluoride-based mixed-anion compounds with sulfide ion. Although some rare earth fluorosulfides have been reported,[6, 7] the reactivity of the compounds requires unique atmospheric control for synthesis.

There are few detailed reports describing the characterization of mixed fluorosulfides. X-ray absorption spectroscopy (XAS) provides information concerning unoccupied orbitals and is a powerful tool for analyzing the electronic structure of compounds. Although fluorine K-edge X-ray absorption near edge structure (XANES) of mixed-anion compounds has been utilized for the analysis of surface layer formation on fluorosulfides,[8] the structure of the XANES spectrum has not been extensively investigated. XANES analysis of fluorosulfide can provide useful information in the development of future applications.

In this study, we analyze the fluorine K-edge XANES of $Ba_{18}F_{18}In_8S_{21}$, which has been reported in the literature[9] and was prepared by solid-state synthesis. The crystal structure has a unique aspect, in which large domains of Ba^{2+} and F^- ions are located in the space between tetrahedral InS_4 and octahedral BaS_6 sites, as shown in Fig. 1. The reported optical band gap was 2.28 eV, [9] which is characteristic of a semiconductor. First-principles calculations yield the density of states (DOS), which allows easy access to information needed for this analysis.[9] Following synthesis of $Ba_{18}F_{18}In_8S_{21}$ by solid-phase reaction and identification of the crystal phase, we conducted fluorine K-edge XANES measurements on the material and compared the results with theoretical calculations.

2. Experimental

Two starting materials were investigated in this study. The first was prepared by mixing BaS:BaF_2:In:S at a 1:1:2:3 mole ratio with a mortar in an Ar-filled

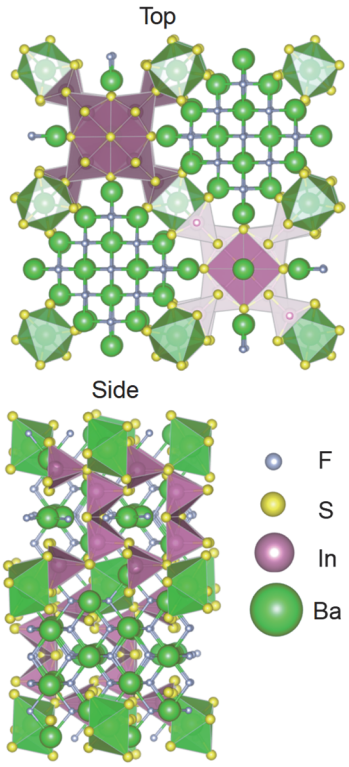

Fig. 1 Crystal structure of $Ba_{18}F_{18}In_8S_{21}$.

glovebox. The second starting material consisted of BaS:BaF_2:In_2S_3 in a 9:9:4 mole ratio. Pellets of the mixtures in a tantalum vessel were vacuum-sealed in a quartz tube and calcined at 800 °C and 700 °C, respectively. The crystal phase of the samples was determined by X-ray diffraction using an Ultima-IV instrument (Rigaku) in 0.02° steps at 40 kV and 40 mA.

Fluorine K-edge XAS measurements were carried out on beamline BL-11 at the Ritsumeikan University SR Center. Powder samples were affixed to a stainless steel holder with carbon tape and measured under vacuum. Spectra were collected in the total-electron yield mode. Energy calibration was performed using the main peak of LiF at 692 eV.

Theoretical XANES investigations of $Ba_{18}F_{18}In_8S_{21}$ were carried out by pseudopotential density functional theory (DFT) code CASTEP using the generalized gradient approximation approach of Perdew-Burke-Ernzerhof (GGA-PBE).[10] The reported crystal structure of $Ba_{18}F_{18}In_8S_{21}$ with lattice parameters a = 22.0703 Å, and c = 12.6143Å was used in the band structure and XANES calculations.[9] Geometry optimization was conducted using the BFGS method to meet the convergence criteria of 2.0×10^{-6} eV/atom for SCF tolerances. A Pulay density mixing scheme was used in the self-consistent-field calculations. The XANES calculations were performed with core-hole treatments by charge removal of a 1s electron from the target atom while smearing a neutralizing charge over the entire system. Calculations of LiF and BaF_2 were also carried out as reference.

3. Results and discussion

XRD patterns obtained from the two kinds of starting materials are shown in Fig. 2 in addition to simulated patterns of $Ba_{18}F_{18}In_8S_{21}$, BaF_2 and In_2S_3. For the synthesis using indium metal and sulfur as starting materials (Fig. 2(a)), pattern #1 is in good agreement with that of the $Ba_{18}F_{18}In_8S_{21}$ target material. However, diffraction patterns #2 and #3 of the samples prepared under identical conditions contain some impurity peaks in addition to those assignable to the diffraction lines of $Ba_{18}F_{18}In_8S_{21}$. The peaks at 24.8, 28.7, 41.4, and 48.6° correspond to the 111, 200, 220, and 311 diffraction peaks of the cubic fluorite structure of BaF_2. This occurs because sulfur, which has a 444 °C boiling point, vaporizes in the quartz tube during calcination. Moreover, indium, which has a 156 °C melting point, is lost by diffusion from the pellet. Therefore, excess BaF_2 is present as an impurity due to deviation from the stoichiometric composition of $Ba_{18}F_{18}In_8S_{21}$. Thus, the synthesis using indium metal and sulfur as starting materials suffers from poor reproducibility.

However, extensive loss of raw material was prevented when In_2S_3, which has a 1050 °C melting point, was used as starting material. XRD patterns #4 and #5 in Fig. 2(b) show the predominant presence of a $Ba_{18}F_{18}In_8S_{21}$ crystalline phase as indicated by the peaks at 24.8°, although a small amount of BaF_2 impurity remains. The BaF_2 content of the starting material was decreased to 90% to prevent formation of residual BaF_2. However, XRD pattern #6 still shows the presence of impurity peaks. Note that any trace of In_2S_3 did not remain at all. The XRD peaks are indexed with the reported $Ba_{18}F_{18}In_8S_{21}$ crystal structure in the tetragonal $P4_2/ncm$ space group. The calculated lattice parameters of a = 22.152(2) Å and c = 12.643(2) Å are in good agreement with the literature[9] and consistent with the formation of $Ba_{18}F_{18}In_8S_{21}$ as the main phase. Control of composition and synthesis over a longer time at higher temperature may succeed in further reducing impurities.

Figure 3(a) shows the DOS obtained by first-principles calculations. The total DOS is in a good agreement with that reported for $Ba_{18}F_{18}In_8S_{21}$.[9] The valence band just below the Fermi level comprises primarily p orbitals with the low-energy side dominated F 2p orbitals and the high-energy side dominated by S 3p orbitals. The bandgap is approximately 2 eV. The In 5s and In 5p orbitals mainly contribute to the low energy part of the conduction band. The higher-energy part comprises

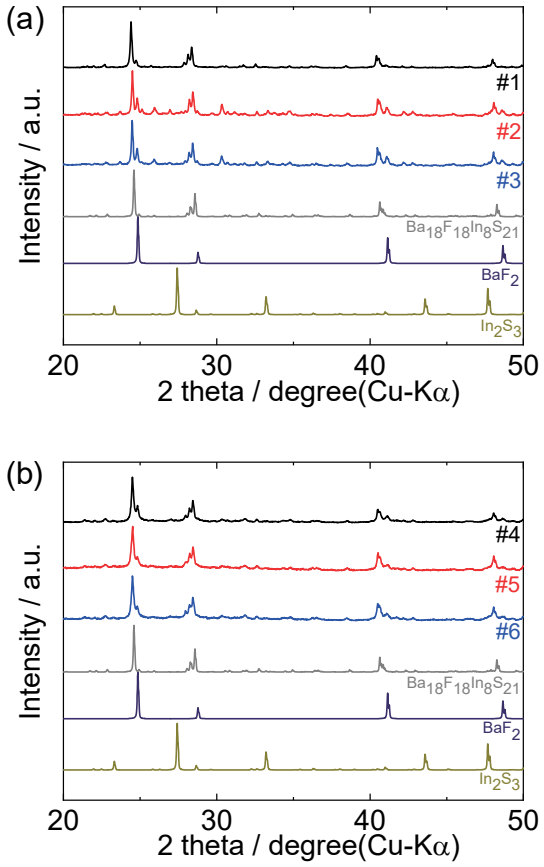

Fig. 2 XRD patterns of $Ba_{18}F_{18}In_8S_{21}$ prepared using (a) In and S and (b) In_2S_3.

primarily d orbitals, wherein the unoccupied Ba 5d orbitals are dominant. The published DOS study states that the conduction band is dominated by unoccupied S 3p, In 5s, and In 5p orbitals.[9] However, the calculations in this work show a clear contribution from d orbitals at approximately 5 eV above the Fermi energy, which differs from the literature report. The calculated partial DOS of fluorine is shown in Fig. 3(b), where it is evident that the unoccupied F 2p orbitals contribute to the conduction band. The fluorine K-edge XANES discussed later reflects transitions from the 1s core orbital to the unoccupied F 2p orbitals. However, due to the core hole-interactions, the provided p-DOS is not equal to XANES spectrum. We performed the theoretical calculation of XANES using the supercell including core-hole.

Figure 4(a) shows the fluorine K-edge XANES spectra of synthesized $Ba_{18}F_{18}In_8S_{21}$ along with those of BaF_2 and LiF for reference. In the spectrum of $Ba_{18}F_{18}In_8S_{21}$, a main peak is observed at 687.5 eV, and other peaks are present at 691 and 694 eV. The XANES profile of BaF_2, on the other hand, shows a sharper main peak at 687.5 eV and a subpeak at 691 eV. The XANES profile of LiF shows a main peak at 692 eV, with the pre-edge peak at 690 eV. Figure 4(b) shows the XANES results obtained by the theoretical calculation. The calculated energy by the reported method [11] was calibrated so as to adjust the main peak of LiF at 692 eV. The calculated XANES profiles are well reproduced, except that of LiF. This is due to the overestimation of the pre-edge peak, which might be overcome by the reconstruction of the LiF supercells. The absorption edge energy differs between LiF and BaF_2 by 4.5 eV, which agrees well with the calculations. Overall profiles seem to be a little bit contracted than the experimental ones and the higher the energy is, the more the peaks shift to the low energy side.

Considering the energy shift for the calculated spectra, the calculated XANES of $Ba_{18}F_{18}In_8S_{21}$ agrees well with the experimental XANES. The calculated XANES shows three broad structures at 687, 688, and 693 eV, which correspond to the peaks at 687.5, 690.5, and 695 eV, respectively, in the experiment. The representative difference of experimental XANES spectra between $Ba_{18}F_{18}In_8S_{21}$ and BaF_2 is the hollow structure at 689 eV. The intensity at this hollow of

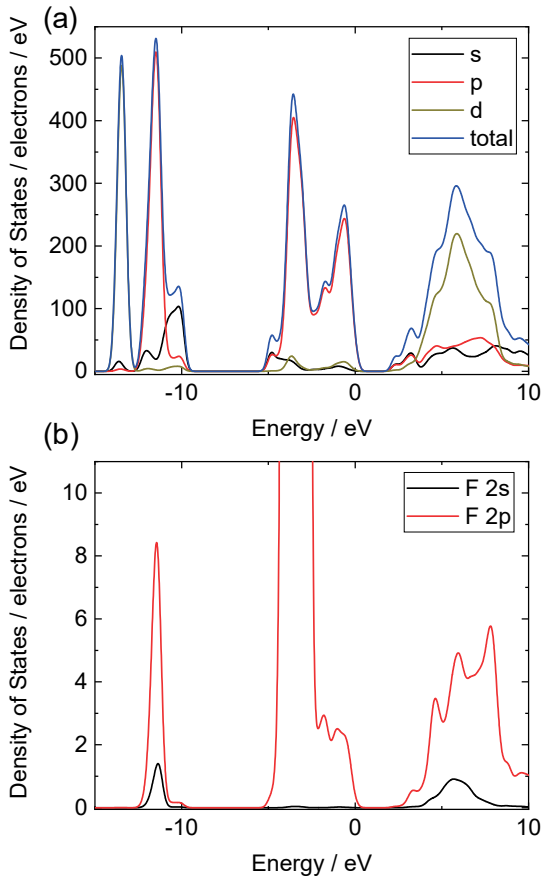

Fig. 3 Density of states of $Ba_{18}F_{18}In_8S_{21}$. (a) and (b) show the total atom and fluorine contributions, respectively.

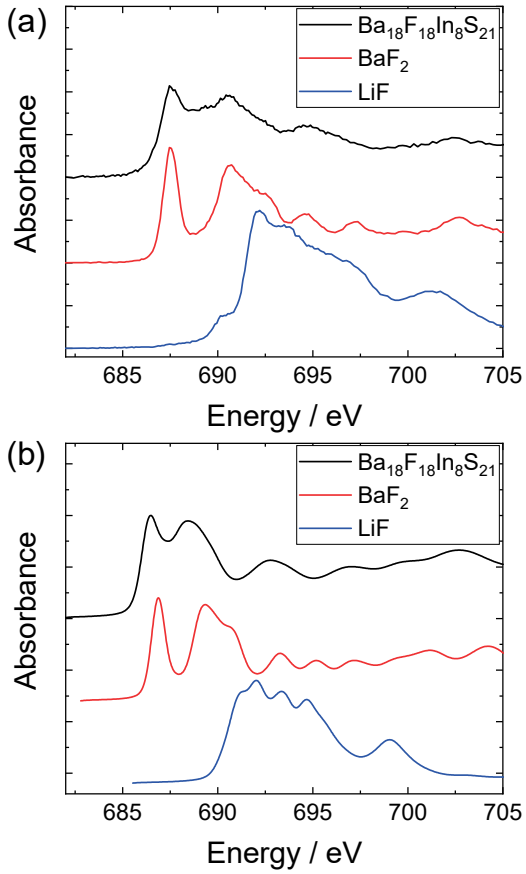

Fig. 4 (a) Fluorine K-edge XANES spectra of synthesized $Ba_{18}F_{18}In_8S_{21}$ with BaF_2 and LiF as references. (b) Calculated XANES spectra of $Ba_{18}F_{18}In_8S_{21}$, BaF_2, and LiF.

BaF_2 is quite small, which is well simulated in the calculated XANES. Despite the energy shift, the fluorine K-edge XANES of mixed-anion fluorosulfides can be reproduced satisfactorily by the theoretical calculations.

4. Conclusion

Solid-state synthesis of the mixed-anion compound, $Ba_{18}F_{18}In_8S_{21}$, is poorly reproducible when indium metal and elemental sulfur are used as starting materials, because of their low melting and boiling point, respectively. Reproducibility of the material is improved by using In_2S_3 in their place. Electronic structural analysis by first-principles calculation shows the $Ba_{18}F_{18}In_8S_{21}$ conduction band to be composed primarily of unoccupied Ba 5d orbitals and partially of unoccupied F 2p orbitals. The fluorine K-edge XANES spectrum shows good agreement with theoretical calculations.

References

(1) H. Kageyama, K. Hayashi, K. Maeda, J.P. Attfield, Z. Hiroi, J.M. Rondinelli, K.R. Poeppelmeier, *Nature Comm.*, **2018**, *9*, 772.
(2) Y. Suemoto, Y. Masubuchi, Y. Nagamine, A. Matsutani, T. Shibahara, K. Yamazaki, S. Kikkawa, *Inorg. Chem.*, **2018**, *57*, 9086-9095.
(3) Q.R. Ding, X.M. Liu, S.G. Zhao, Y.S. Wang, Y.Q. Li, L.N. Li, S. Liu, Z.S. Lin, M.C. Hong, J.H. Luo, *J. Am. Chem. Soc.*, **2020**, *142*, 6472-6476.
(4) G.Y. Gou, M. Zhao, J. Shi, J.K. Harada, J.M. Rondinelli, *Chem. Mater.*, **2020**, *32*, 2815-2823.
(5) M. Leblanc, V. Maisonneuve, A. Tressaud, *Chem. Rev.*, **2015**, *115*, 1191-1254.
(6) P.O. Andreev, O.G. Mikhalkina, O.V. Andreev, A.V. Elyshev, *Russ. J. Phys. Chem. A*, **2015**, *89*, 731-736.
(7) H. Grossholz, I. Hartenbach, G. Kotzyba, R. Pottgen, H. Trill, B.D. Mosel, T. Schleid, *J. Solid State Chem.*, **2009**, *182*, 3071-3075.
(8) S. Tachibana, H. Yamagishi, Y. Orikasa, *Memoirs of the SR Center Ritsumeikan University*, **2019**, *21*, 7-9.
(9) Z.-Z. Luo, C.-S. Lin, W.-L. Zhang, H. Zhang, Z.-Z. He, W.-D. Cheng, *CrystEngComm*, **2014**, *16*, 2788-2794.
(10) S.J. Clark, M.D. Segall, C.J. Pickard, P.J. Hasnip, M.J. Probert, K. Refson, M.C. Payne, *Zeitschrift für Kristallographie*, **2005**, *220*, 567-570.
(11) T. Mizoguchi, I. Tanaka, S.-P. Gao and C. J. Pickard, *J. Phys.: Condens. Matter*, **2009**, *21*, 104204.